THE JOURNAL OF PHYSICAL CHEMISTRY B
A JOURNAL OF THE AMERICAN CHEMICAL SOCIETY

pubs.acs.org/JPCB

Article

Evaluating the Conformations and Dynamics of Peptoid Macrocycles

James R. B. Eastwood, Linhai Jiang, Richard Bonneau, Kent Kirshenbaum,* and P. Douglas Renfrew*

Cite This: *J. Phys. Chem. B* 2022, 126, 5161−5174

Read Online

ACCESS | Metrics & More | Article Recommendations | Supporting Information

ABSTRACT: Peptoid macrocycles are versatile and chemically diverse peptidomimetic oligomers. However, the conformations and dynamics of these macrocycles have not been evaluated comprehensively and require extensive further investigation. Recent studies indicate that two degrees of freedom, and four distinct conformations, adequately describe the behavior of each monomer backbone unit in most peptoid oligomers. On the basis of this insight, we conducted molecular dynamics simulations of model macrocycles using an exhaustive set of idealized possible starting conformations. Simulations of various sizes of peptoid macrocycles yielded a limited set of populated conformations. In addition to reproducing all relevant experimentally determined conformations, the simulations accurately predicted a cyclo-octamer conformation for which we now present the first experimental observation. Sets of three adjacent dihedral angles (ϕ_i, ψ_i, ω_{i+1}) exhibited correlated crankshaft motions over the course of simulation for peptoid macrocycles of six residues and larger. These correlated motions may occur in the form of an inversion of one amide bond and the concerted rotation of the preceding ϕ and ψ angles to their mirror-image conformation, a variation on "crankshaft flip" motions studied in polymers and peptides. The energy landscape of these peptoid macrocycles can be described as a network of conformations interconnected by transformations of individual crankshaft flips. For macrocycles of up to eight residues, our mapping of the landscape is essentially complete.

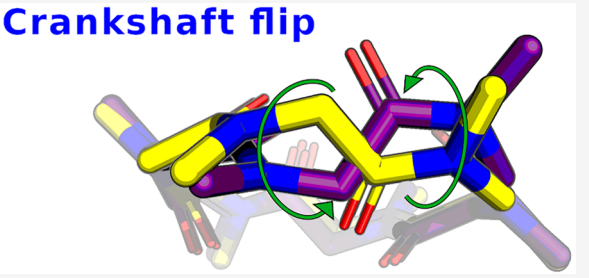

INTRODUCTION

Peptide macrocycles, along with other cyclic oligomers, promise a solution to one of the great challenges of drug design, the modulation of protein−protein interactions,[1] and are being pursued as therapeutics to address many significant health threats of our era.[2,3] *N*-Substituted glycine oligomers, termed "peptoids," are a family of peptidomimetics that offer ready access to enormous side chain diversity through a simple solid phase synthesis route, in addition to improved cell permeability and protease resistance compared to their analogous peptides. Head-to-tail cyclization of peptoid oligomers further improves cell permeability[4] and has been used extensively to enforce conformational order in peptoids since the first report of cyclic peptoids over a decade ago.[5,6] Cyclic peptoids have been used as mimics of naturally occurring macrocycles[7] and as de novo inhibitors of protein−protein interactions.[1] Further development of rational design techniques for bioactive cyclic peptoids will depend on the ability to establish control over the three-dimensional conformations of the macrocycles. A more detailed understanding of their conformational energy landscape is necessary to guide this effort. Techniques for the generation of macrocycle conformers remain an active field of development in computational chemistry,[8−16] and computational studies of macrocycle interactions with protein surfaces have been shown to benefit from careful treatment of the constrained flexibility of the backbone.[2,17] Moreover, peptoid macrocycles provide a model system in which to study the behavior of turn conformations, which will comprise critical elements in future designs of peptoid tertiary structures. Therefore, peptoid macrocycle conformations merit careful study.

As reviewed in detail by D'Amato et al., cyclic peptoids exhibit several forms of stereoisomerism.[18] The energetic barrier to inversion of the amide bond leads to a range of configurational (cis−trans) isomers that interconvert, under ambient conditions, on a time scale between that of NMR (1×10^{-6} s) and chemical separation (1×10^{3} s).[19] Moreover, the achiral α-carbon of peptoids produces a symmetrical energy landscape with respect to the ϕ and ψ torsions (Scheme 1),[20] resulting in twice as many conformational isomers as would be obtained for a comparable chiral oligomer. This conformational lability has made linear peptoid structures challenging to characterize. Cyclization imposes conformational restrictions on the peptoid backbone, often facilitating crystallization and structure determination. NMR studies of cyclic peptoids in solution, however, often reveal a conformational ensemble.[21]

Received: March 9, 2022
Revised: May 26, 2022
Published: July 12, 2022

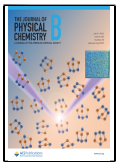

Scheme 1. Conformational Features of Sarcosine

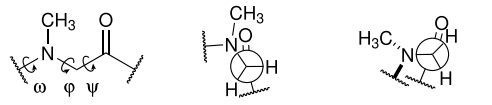

N-methylglycine Sarcosine "Sar" | Z (φ=±75°, ψ=180°) | $C_{7\beta}$ (φ=±130°, ψ=±75°)

X-ray crystallographic studies establish that, for a given macrocycle size, more than one of these conformations can be stabilized within the solid state,[22−24] with the structures appearing to depend on the side chain functional groups and additional influences from counterions. It is worth noting that all previously observed crystal structure conformations of cyclic peptoids with even numbers of residues (the preponderance of all cyclic peptoids crystallized) contain an element of two-fold rotational symmetry within each molecule. The prevalence of symmetric structures suggests that they are favored during crystallization events, implying that additional, asymmetric, low-energy conformations may dominate in solution. Finally, the directionality of the backbone leads to an element of planar chirality upon cyclization, as left-handed and right-handed cyclizations form an enantiomeric pair and can lead to a profusion of diastereomers (or atropisomers) in a molecule containing chiral side chains.[25] Many of the solved crystal structures of cyclic peptoids contain an inversion center symmetry element, only possible in a racemic mixture or a symmetric molecule. Due to these many subtle stereochemical features, the energy landscape of cyclic peptoid conformations is highly complex.

As mentioned, experimental studies of cyclic peptoids have identified a number of distinct conformations in the solid phase, including two novel structures reported after the initiation of this work[23,24] and a third reported here. Voelz et al. have previously demonstrated a method using the Generalized Amber Force Field (GAFF) in molecular dynamics (MD) simulations that reproduces experimental structures[26] and successfully predicted the conformation of a novel cyclic peptoid nonamer.[27] Several researchers have used enhanced sampling techniques in MD simulations, along with NMR data, to predict structures of cyclic peptides and peptidomimetics.[28−30] More recently, the Rosetta macromolecular modeling suite has been used to exhaustively sample the conformational space of cyclic peptides, developing design tools that facilitate the stabilization of individual conformations for experimental characterization.[31] We sought to correlate the experimental results on cyclic peptoids with simulated ensembles in a way that could guide design efforts by providing sets of conformations (representing accessible backbone geometries) that might be stabilized by particular side chain sequences.

A recent review of the peptoid folding landscape has shown that peptoid monomer units favor only four conformations (two symmetric pairs), rather than the six previously predicted;[32−34] therefore we hypothesize that the landscape of cyclic conformations may be navigable by some "shortcut," a simple rule that describes the relationship, in geometric space, between the important energy wells. MD simulations of small cyclic peptides have shown that conformational conversions occur via two pathways, each of which is a concerted, large-scale dihedral angle motion: one between adjacent ϕ and ψ angles, and one between ψ on one residue and ϕ on the following residue.[35] This second motion, which results in the rotation of an amide plane by approximately 180°, is a peptide-specific example of a motion known as a "crankshaft flip", which has been studied in Monte Carlo simulations of polymers since the 1970s.[36] The crankshaft flip has been observed directly in crystal structures of antibody loops,[37] and has recently been used to define collective variables for Metadynamics simulations of cyclic peptides.[38] Smaller crankshaft motions of this same pattern have been correlated with experimental observables from NMR.[39] We find here that a related crankshaft flip in cyclic peptoids is a sufficient shortcut to sample many of their distinct conformations. This shortcut enables the set of populated conformations to be viewed as a network densely connected by crankshaft flips. Our mapping of the landscape, guided by this shortcut, is essentially complete for peptoid macrocycles of up to eight residues.

METHODS

Experimental Section. *Materials.* *N*,*N*′-Diisopropylcarbodiimide (DIC) was purchased from Alfa Aesar. Dichloromethane (DCM), acetonitrile (ACN) and HPLC grade water were supplied by Pharmco. 2-Chlorotrityl chloride resin, *N*,*N*-diisopropylethylamine (DIEA), trifluoroacetic acid (TFA), 2,2,2-trifluoroethanol (TFE), acetic acid, triisopropylsilane (TIPS), bromoacetic acid (BrAA), *N*,*N*-dimethylformamide (DMF), *N*-methyl-2-pyrrolidone (NMP), potassium hydroxide, rubidium hydroxide, and PyBOP were purchased from Millipore Sigma. Glycine *tert*-butyl ester hydrochloride was purchased from Chem-Impex. Deionized water was produced in the lab by an Elga water purification system.

Synthesis of Ncm6 and Ncm8. The linear precursors were synthesized through submonomer solid phase synthesis methods using 2-chlorotrityl chloride resin as the solid support. The following procedure is optimized for a synthesis scale of 200 mg resin with a loading number of 1.4 mmol/g. Prior to synthesis, the resin was swelled in DCM for 45 min. The first residue was added through (1) 45 min shaking of the resin in the mixture of 2 mL of 0.65 M BrAA/DCM solution and 0.216 mL of DIEA and (2) 20 min shaking in 2 mL of 1.4 M glycine *tert*-butyl ester/NMP solution. The coupling of the remaining peptoid residues was carried out by iterative steps of (1) 20 min shaking of the resin in the mixture of 2 mL of 1.2 M BrAA/DMF solution and 0.4 mL of DIC and (2) 20 min shaking with 2 mL of 1.4 M glycine *tert*-butyl ester/NMP solution. The resin was washed by DMF thoroughly after each step. Mild cleavage of the linear precursor from the solid support was achieved by using 5 mL cleavage cocktail composed of 10 vol % acetic acid, 10 vol % TFE, and 80 vol % DCM. After being shaken for 1 h, the solution was dried by using nitrogen gas flow. The resulting oily product was dissolved in a water/acetonitrile (50:50 by volume) cosolvent. Three cycles of dissolution-lyophilization were performed for complete removal of residual acetic acid. The lyophilized powder was used for cyclization without any intermediate purification.

The glycine *tert*-butyl ester was prepared as the free base in NMP solution as follows: (1) the as-received powder (glycine *tert*-butyl ester hydrochloride) was directly dissolved in NMP at a concentration of 1.4 M; (2) 0.95 equiv of KOH (11 M aqueous solution) was added to the solution to neutralize the HCl; and (3) the precipitated KCl pellets were separated by centrifugation, and the supernatant was then used for the synthesis of linear peptoids.

https://doi.org/10.1021/acs.jpcb.2c01669
J. Phys. Chem. B 2022, 126, 5161−5174

The cyclization reactions of the linear oligomer precursors were conducted following a procedure we previously reported.[5] A 0.5 mM linear peptoid solution was prepared by dissolving the lyophilized powder of linear precursor in the proper amount of dry DCM, followed by the addition of 6 equiv DIEA and 3 equiv PyBOP. The reaction mixture was stirred for 12 h under nitrogen gas at 25 °C. Afterward, DCM was removed by rotary evaporation. The cyclized products were purified by reverse-phase HPLC using water and ACN as mobile phases. The purified HPLC fractions were then lyophilized for 3 days. The lyophilized powder was then dissolved in a deprotection cocktail containing 95 vol % TFA, 2.5 vol % TIPS, and 2.5 vol % water to remove the *tert*-butyl protecting groups. After 3-h shaking, the solution was dried by using nitrogen gas flow. The resulting oily product was dissolved in a water/acetonitrile (50:50 by volume) cosolvent and purified again by reversed phase HPLC using water and ACN as mobile phases. The purified HPLC fractions were then lyophilized for 3 days. The molecular weight of each product was confirmed by using Agilent 6120 single quadrupole LC−MS spectrometer (Figure S1 of the Supporting Information, SI).

Preparation of Single Crystals. The single crystals studied by X-ray crystallography in this work were prepared as follows: The lyophilized cyclic peptoid powder was dissolved in the proper amount of basic aqueous solution (600 mM KOH for compound **Ncm6** and 800 mM RbOH for compound **Ncm8**) to reach a concentration of 0.1 M and pH value of 7.5. Crystals were obtained by slow evaporation at 25 °C.

X-ray Crystallography. *Ncm6.* A colorless plate-like specimen of $C_{24}H_{50}K_6N_6O_{31}$, with approximate dimensions 0.060 × 0.210 × 0.410 mm^3, was used for the X-ray crystallographic analysis. The X-ray intensity data were measured on a Bruker APEX-II CCD system equipped with a graphite monochromator and a Mo sealed tube (λ = 0.71073 Å).

A total of 2000 frames were collected at 295 K. The total exposure time was 22.22 h. The frames were integrated with the Bruker SAINT software package using a narrow-frame algorithm. The integration of the data using a triclinic unit cell yielded a total of 39 512 reflections to a maximum θ angle of 26.40° (0.80 Å resolution), of which 9537 were independent (average redundancy 4.143, completeness = 99.9%, R_{int} = 2.95%, R_{sig} = 2.72%) and 7370 (77.28%) were greater than 2σ(F2). The final cell constants of a = 10.2999(7) Å, b = 13.7601(10) Å, c = 17.4871(12) Å, α = 87.116012°, β = 88.7715(12)°, γ = 70.0334(12)°, and volume = 2326.5(3) $Å^3$, are based upon the refinement of the XYZ-centroids of 9985 reflections above 20 σ(I) with 4.801° < 2θ < 52.67°. Data were corrected for absorption effects using the multiscan method (SADABS). The ratio of minimum to maximum apparent transmission was 0.881. The calculated minimum and maximum transmission coefficients (based on crystal size) are 0.6567 and 0.7454.

The structure was solved and refined using the Bruker SHELXTL Software Package, using the space group P −1, with Z = 2 for the formula unit, $C_{24}H_{50}K_6N_6O_{31}$. The final anisotropic full-matrix least-squares refinement on F2 with 737 variables converged at R_1 = 4.47%, for the observed data and wR_2 = 12.54% for all data. The goodness-of-fit was 1.049. The largest peak in the final difference electron density synthesis was 0.777 $\frac{e^-}{Å^3}$ and the largest hole was −0.692 $\frac{e^-}{Å^3}$ with an RMS deviation of 0.057 $\frac{e^-}{Å^3}$. On the basis of the final model, the calculated density was 1.646 g/cm^3 and F(000), 1196 e^-. The structure has been deposited in the Cambridge Structural Database under Deposition Number 2153121.

Ncm8. A colorless plate-like specimen of $C_{32}H_{65.61}N_8O_{40.81}Rb_8$, with approximate dimensions 0.110 × 0.290 × 0.370 mm^3, was used for the X-ray crystallographic analysis. The X-ray intensity data were measured on a Bruker D8 SMART APEXII three-circle diffractometer system equipped with a Incotec microfocus sealed X-ray tube (MoKα, λ = 0.71073 Å) and a multilayer optics monochromator. A total of 2402 frames were collected. The total exposure time was 18.72 h. The frames were integrated with the Bruker SAINT software package using a narrow-frame algorithm. The integration of the data using a monoclinic unit cell yielded a total of 154 449 reflections to a maximum θ angle of 26.42°(0.80 Åresolution), of which 13204 were independent (average redundancy 11.697, completeness = 99.7%, R_{int} = 8.61%, R_{sig} = 4.53%) and 11042 (83.63%) were greater than 2σ(F2). The final cell constants of a = 37.118(2) Å, b = 10.6979(7) Å, c = 37.004(3) Å, β = 118.8372(17)°, and volume = 12871.6(16) $Å^3$ are based upon the refinement of the XYZ-centroids of 9135 reflections above 20 σ(I) with 5.026° < 2θ < 52.77°. Data were corrected for absorption effects using the Multi-Scan method (SADABS). The ratio of minimum to maximum apparent transmission was 0.514. The calculated minimum and maximum transmission coefficients (based on crystal size) are 0.2100 and 0.5520. The element analysis results from electron dispersive spectroscopy were used to assist the structure refinement. The structure was solved and refined using the Bruker SHELXTL Software Package, using the space group C12/c1, with Z = 8 for the formula unit, $C_{32}H_{65.61}N_8O_{40.81}Rb_8$. The final anisotropic full-matrix least-squares refinement on F2 with 963 variables converged at R_1 = 6.07%, for the observed data and wR_2 = 18.17% for all data. The goodness-of-fit was 1.066. The largest peak in the final difference electron density synthesis was 2.111 $e^-/Å^3$ and the largest hole was −1.547 $e^-/Å^3$ with an RMS deviation of 0.188 $e^-/Å^3$. On the basis of the final model, the calculated density was 1.960 g/cm^3 and F(000), 7488 e^-. The structure has been deposited in the Cambridge Structural Database under Deposition Number 2153125.

Computational. *Model Generation.* Starting models ("seeds") were constructed in PyRosetta as oligomers of *N*-methyl glycine. For each macrocycle size, the complete set of unique patterns of *cis*- and *trans*- amide bonds was modeled, with each of these patterns generating two seed conformations. The oligomer ω angles were idealized at 0° (cis) and 180° (trans), and ψ idealized at 180°. The entire combinatorial space of idealized ϕ angles (±70°) was explored, with each combination being subjected to a backbone minimization (over the Rosetta Energy Function[40]) to enforce the loop closures required to form cyclic structures. These conformations were scored using the Rosetta Energy Function, and the lowest-scoring conformation was selected. Each of these selected conformations was then inverted to generate the enantiomeric pair.

MD Simulation. A dipeptoid model of the sarcosine monomer was prepared by Geometry Optimization in Gaussian '09.[41] Next, AM1-BCC charge fitting for GAFF atom type assignment was performed on this dipeptoid model.[42] Then the atom types from this model were assigned to the *N*-methyl glycine residues from the PyRosetta-generated seeds. These "seed" conformations were minimized with GAFF

https://doi.org/10.1021/acs.jpcb.2c01669
J. Phys. Chem. B 2022, 126, 5161−5174

in conjunction with the Generalized Born/Surface Area implicit solvent model. The GAFF-minimized seeds were each subjected to a short heating trajectory using the OBC implementation of the Generalized Born/Surface Area implicit solvation model,[26] followed by 5 independent 20 ns trajectories at 300 K.

Trajectory Analysis. Trajectories were evaluated by comparing the dihedral space sampled to the experimental results from known peptoids.[20] Circular correlation coefficients were calculated over all frames of all trajectories for each pair of backbone dihedral angles, using the definition provided by Jammalamadaka:[43]

$$\rho_c(\alpha, \beta) = \frac{E\{\sin(\alpha - \mu)\sin(\beta - \mu)\}}{\sqrt{\mathrm{Var}(\sin(\alpha - \mu))\mathrm{Var}\,(\sin(\beta - \mu))}} \quad (1)$$

Trajectories were clustered by binning dihedral space for each backbone bond into quadrants (centered on 0°, 90°, 180°, −90°). Each unique sequence of dihedral bins was defined as a conformation. Conformations populated by fewer than $1/10^{th}$ the number of frames of the largest cluster were discarded.

A crankshaft flip relationship was defined as two conformations differing by only two bins, for which the two differing bins correspond to the hypothesized move (ϕ_i, ω_{i+1}). Each conformation's bin sequence was compared to the set of bin sequences defined by individual crankshaft flips from each other conformation. Conformation energies were reported as the Total Potential Energy as calculated by GAFF.

Simulation of Transition Pathway. The transition pathway between the **tttttt** and **cttctt** hexamer backbones, as observed in the cited crystal structure,[24] was simulated using the Swarm-of-Trajectories String Method as reported by Pan et al.[44] and implemented in Amber18[45] as part of the Adaptively-Biased Molecular Dynamics (ABMD) free energy methods suite. The exemplar structure corresponding to the all-*trans*-amide hexamer was used as the starting conformation. A Steered Molecular Dynamics simulation was performed, with two opposite ω torsions defined as Collective Variables (CV). The first CV was steered from π to 0 over 500 ps, and the second CV over the following 500 ps. The harmonic constant of the first was set to 10 kcal/mol/rad^2 for the first 500 ps, after which it was decreased to 1.0 kcal/mol/rad^2, while the second was increased from 1.0 to 10.0 over the first 500 ps. This steering was chosen from several alternatives (see Table S2).

The Steered MD trajectory was sampled into 16 evenly spaced frames, each of which was equilibrated in a Pinned MD simulation with harmonic potential set to 1000 kcal/mol/rad^2 for 100 000 frames. These equilibrated trajectories were then taken as input images to the Swarm-of-Trajectories simulation. Each of the 16 images was simulated in 16 independent trajectories, restrained for 980 frames, and then allowed to release for 20 frames. The average drift of these 16 trajectories in CV space was calculated, and the string of resulting centers was interpolated and smoothed to create a new transition path. Sixteen new restraint values were evenly spaced along this new curve, and used to restrain the images for the next iteration of the method. The simulation was repeated for 30 iterations. The resulting 16 images were clustered according to the same strategy used previously. The resulting number of clusters along the transition pathway was compared to results from String Method simulations based on several alternative CV schemes; the steering described here was chosen for producing the smallest number of clusters in the final transition pathway.

RESULTS

A recent review of high-resolution peptoid structures reveals that almost all residues in solved structures fall into one of four conformations,[20] denoted the *Z* conformations, Z_{Rc}, Z_{Rt}, Z_{Sc}, or Z_{St}, corresponding to the *cis*- and *trans*-amide bond configurations combined with right- or left-handed orientation of one amide plane with respect to the next. The empirical results defining the *Z* conformations agree well with the earliest understanding of the conformational preferences of cyclized oligomers of sarcosine;[46] therefore, we used cyclic sarcosine oligomers with ring sizes of 12−27 atoms (compounds **Sar4**−**Sar9**) as a model system (Chart 1) to study the range of conformations accessible to cyclic peptoids.

Chart 1. Molecules Simulated

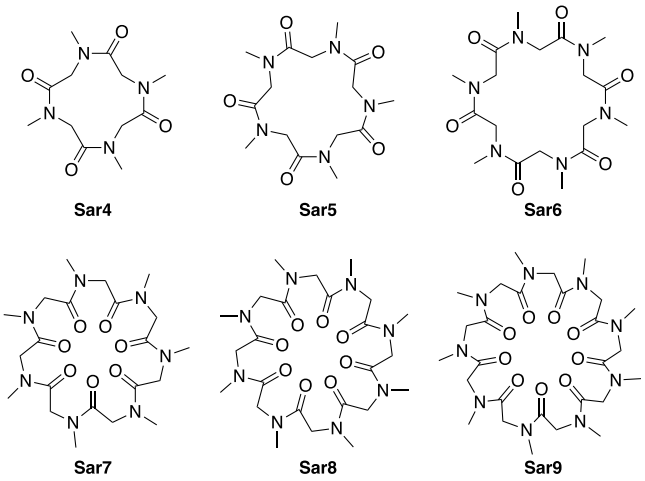

In the well-studied peptoid macrocycles of six or eight residues, as in almost all linear peptoid oligomers, the ϕ dihedral can adopt two mirror-image conformations around ±75°, while the ψ dihedral falls into a single, broad energy well centered around 180°. This set of conformations, enumerated in Table 1, are defined as the *Z* conformations.

Table 1. Dihedral Angles of Idealized *Z* Conformations

	ω	ϕ	ψ
Z_{Rt}	180°	75°	180°
Z_{St}	180°	−75°	180°
Z_{Rc}	0°	75°	180°
Z_{Sc}	0°	−75°	180°

An alternative conformation ($\phi \sim \pm 130°$, $\psi \sim \pm 75°$), known for historical reasons as $C_{7\beta}$[47,48] (see Scheme 1), is observed primarily in small macrocycles,[49−53] where it is understood to be induced by ring strain.[46] Theoretical studies predict that a sarcosine monomer may also adopt the conformation corresponding to a peptide α-helix, but this conformation has not been observed in experimental structures. In macrocycles larger than 4 residues, no conformation has been experimentally discovered that involves more than one residue out of a *Z* conformation. Therefore, we used these four idealized *Z* conformations to guide our conformational modeling process, and began by using Rosetta to explore the landscape defined by all possible combinations of the *Z* conformations at each residue.

https://doi.org/10.1021/acs.jpcb.2c01669
J. Phys. Chem. B 2022, 126, 5161−5174

From prior knowledge that the amide bond interconversion is the slowest individual conformational change,[19,54] we built two mirror-image approximate low-energy conformations for each unique pattern (taking cyclic symmetry into account) of amide bond configurations. These starting models ("seeds") were built using Rosetta, where, for a given amide bond pattern, all possible combinations of left- and right-handed Z conformations were subjected to a chainbreak-closing minimization, and the lowest-scoring model, along with its mirror image, was selected. In order to gain some dynamic insight into these conformations, and because the Rosetta all atom energy function has not been evaluated for its ability to reproduce accurate peptoid structures, we used these seeds to initiate equilibrium MD simulations following the methods of Voelz et al.[26] The Rosetta models were minimized with GAFF[42] and simulated in Amber using the Generalized Born[55] implicit solvent model at 300 K for a total of 100 ns for each amide bond pattern to explore the local conformational energy landscape. We were more concerned with the geometry of the local energy minima than with their relative free energy, since careful selection of side chains will alter the energetics of the landscape but will not significantly alter the backbone geometry at these minima. For this reason, we concluded that simulating each amide bond pattern as a distinct chemical entity (without accelerating interconversions between them; see Table S1) was a prudent strategy for obtaining the desired data.

Sampling. Sampling results were evaluated by comparing the dihedral space sampled by the simulations to the Ramachandran-style maps published by Spencer et al.,[20] as well as directly to experimental structures of the relevant peptoid macrocycles. See Figures 1, 2A, and S2−S4 for histograms of backbone dihedral angle sampling.

Tetramer. Peptoid cyclo-tetramers are known to populate a single conformation, both in the solid state and in solution,[21,23,49,56,57] with alternating *cis*- and *trans*-amide bonds and two opposite residues adopting the Z conformation while the other two adopt the $C_{7\beta}$ conformation. These conformations are clearly visible in the sampling results for the cyclo-tetramer, shown in Figure 1. Sampling any other pattern of bond dihedrals is expected to produce highly distorted structures that may have no available relaxation pathway over the 100 ns time scale of the simulation. Indeed, our simulations of **Sar4** sampled severely twisted amide bonds[5] and ϕ/ψ distributions significantly more complex than in the four-well model. These results demonstrate one limitation of this sampling strategy: we greatly oversample the landscape of this tightly constrained molecule without lowering the energy barriers to conformational conversion. We have included the tetramer results to illustrate that pentamers are the smallest peptoid molecule which can be accurately studied with this idealized model.

Pentamer. Cyclic pentapeptoids show some flexibility in solution-phase experiments and mostly Z backbone conformations in the solid phase.[50,53] Two pentapeptoid molecules (including pentasarcosine) have been solved by X-ray diffraction, and both adopt the same backbone conformation with one residue adopting $C_{7\beta}$. A similar pattern is observed in these simulation results of **Sar5**: $C_{7\beta}$ comprises approximately 20% of sampled dihedral space, and the most-populated clusters contain a single residue in this conformation (see Figures 2B,C and S2, and discussion of clustering results, vide infra). Moreover, X-ray crystal structures of cyclopentamers

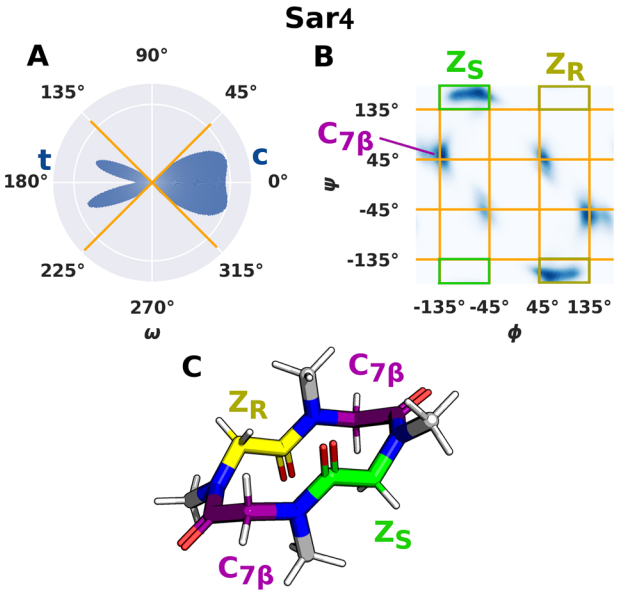

Figure 1. Backbone sampling results for **Sar4**, with conformations labeled and illustrated. Orange lines indicate bin boundaries used for clustering. (A) ω angle sampling presented as a polar histogram. Sampled states in both amide configurations are severely distorted from planarity (values of 0° or 180°) for this small macrocycle. (B) ϕ vs ψ angle sampling presented as a Ramachandran plot. Sampled states include all six theoretical conformations of sarcosine as a result of both ring strain and significant oversampling. Bin boundaries capture Z conformations, which are the major populated conformations in larger macrocycles. (C) Model illustrates labeled conformations, with carbon atoms colored to match the label Z_S (green), Z_R (yellow), $C_{7\beta}$ (purple).

show amide bonds distorted from planarity by up to 18°, while the amide bond dihedrals sampled in these simulations formed a broad, bimodal distribution centered approximately 30° off of planar.

Hexamer. Amide bond sampling in **Sar6** splits into two symmetrical twisted variations on the trans configuration (Figure 2A). This bimodal twisted trans configuration poses an interesting comparison with X-ray crystal structures of cyclic peptoids, which contain amide bonds approximately 15° out-of-plane, but with *cis*-amide bonds more twisted than *trans*-amide.[5] Sampling of the ϕ and ψ dihedrals in **Sar6** converges on the Z conformation, with minimal sampling of alternative residue conformations.

Heptamer. Simulations of **Sar7** sample bond dihedrals that are predominantly in the Z conformation (see Figures 2B and S3), with a notable exception: the conformation ranked lowest in potential energy contains one $C_{7\beta}$ residue, in agreement with the X-ray crystal structure of the same molecule[51] (see Table 2).

Octamer and Nonamer. Simulations of **Sar8**, **Sar9** produce nearly planar amide bond sampling, and virtually no sampling of ϕ, ψ dihedrals outside of the Z conformation, as shown in Figures 2A,B and S4.

Clustering. On the basis of the observation that the distributions of each dihedral angle fell neatly within quadrants of the polar axis (offset by 45°; see Figure 2), and on the previously discussed simplicity of the expected energy landscape inhabited by each residue, trajectories were clustered by binning dihedral space for each backbone bond into quadrants, and a designation assigned to each residue

https://doi.org/10.1021/acs.jpcb.2c01669
J. Phys. Chem. B 2022, 126, 5161−5174

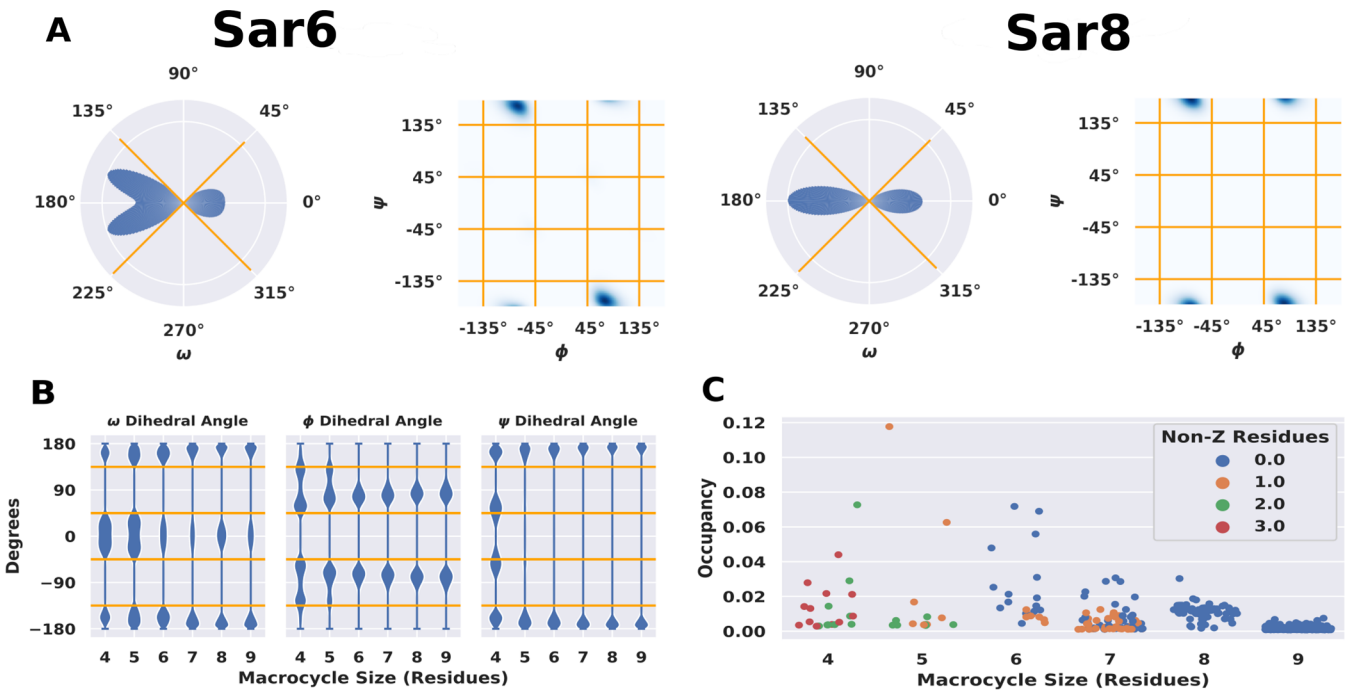

Figure 2. Backbone dihedral angle preferences of residues in each macrocycle size. As macrocycle size increases, populations of clusters trend toward the behavior of an unstructured oligomer, with many equally populated clusters and virtually all residues in the *Z* conformation. (A) ω (polar representation) and ϕ vs ψ (Ramachandran representation) histograms for molecules of even-numbered residues (see SI for corresponding histograms for molecules of odd-numbered residues). (B) Violin plot of backbone dihedral angles sampled over all residues in all MD trajectories of each macrocycle size. Width of the plot corresponds to the normalized kernel density estimate. Orange lines in A,B indicate the bin boundaries used for clustering. Simulations of **Sar4** and **Sar5** sampled nonideal geometries that crossed bin boundaries; larger macrocycle sizes converged on ideal *Z* conformations. (C) Conformational clusters studied in each macrocycle size. Y-position represents the fraction of total trajectory frames in the cluster. Color represents number of residues in nonideal local conformations.

Table 2. Comparison between X-ray Crystal Structures and Conformations Identified in the Simulations Performed in This Study

cycle size	amide pattern[a]	# experimental structures	RMSD[b] (Å)	refs
4	**ctct**	6	0.143	23, 49, 56, 57
5	**ccctt**	2	0.270	50,53
6	**tttttt**	4	0.189	7,22,24,56
	cttctt	1	0.266	24
	cctcct	11	0.263	5,7,22,23,58−63
7	**ccccttt**	1	0.228	51
8	**ccttcctt**	4	0.443	5,64−67
	ctctctct	1	0.435	23
	cttttttt	1	0.402	this work

[a]**c** denotes *cis*-amide, **t** denotes *trans*-amide bond. [b]RMSD calculated over backbone heavy atoms between cluster exemplar and representative crystal structure

according to which of the four *Z* conformations was populated. Quadrants expected to be unpopulated were combined into a single bin for each dihedral, to characterize a bond dihedral as "non-Z". The configuration of the amide bond has heretofore been used as the defining feature of cyclic peptoids, with overall conformations denoted as patterns of **c** and **t** (shorthand for *cis*- and *trans*-amides). The *Z* nomenclature expands on this amide pattern notation by additionally reporting that the residue is in the expected region of Ramachandran space and which mirror-image conformer is adopted (that is, **tttttt** corresponds to $Z_{Rt}Z_{St}Z_{Rt}Z_{St}Z_{Rt}Z_{St}$ and its mirror image $Z_{St}Z_{Rt}Z_{St}Z_{Rt}Z_{St}Z_{Rt}$; **cttctt** corresponds to $Z_{Rc}Z_{St}Z_{St}Z_{Sc}Z_{Rt}Z_{Rt}$ and its mirror image).

After trajectories were clustered in this way, it was observed that most clusters contained very few frames, and the majority of frames populated a few favored clusters. The sampling strategy used treated each amide bond pattern as a distinct chemical entity and each was simulated for the same number of frames, so we expected local minima of each seed to be represented by a comparable number of frames if the seed represents a point on the landscape near to a local minimum. Therefore, clusters containing less than $1/10^{th}$ the population of the most-populated cluster were assumed to be transition states and deemed trivial. The nontrivial clusters were merged by their symmetry operations, eliminating artificial distinctions between cyclic permutations of the same conformation, then ranked by the minimum single-point GAFF energy (corresponding to total potential energy of the molecular conformation) of any frame in the cluster. It is noteworthy that none of the observed conformations for the hexamer or

https://doi.org/10.1021/acs.jpcb.2c01669
J. Phys. Chem. B 2022, 126, 5161−5174

larger macrocycles contained more than one residue out of the Z conformation, as evident in Figure 2C. For the hexamer, the several most prevalent conformations contained only Z residues, and for the octamer only a single conformation contained a residue out of Z. For each conformational cluster, the simulation frame with lowest potential energy (according to single-point GAFF calculation) was chosen to exemplify the conformation, for comparison with experimental structures. These exemplar structures are available in PDB format as SI.

Comparison to Experimental Results. The cluster exemplars included very close matches to all experimentally determined peptoid macrocycle structures of up to eight residues, as shown in Table 2. Several of the experimentally observed solid-state conformations have been identified in numerous structures with different side chains (see the "# experimental structures" column of Table 2), with root-mean-squared deviation close to or below the resolution limit of the X-ray structures. The simulation exemplars for macrocycles smaller than eight residues match these conformations to a similar precision. Only one cyclononamer crystal structure has been determined,[27] and a corresponding conformation was not found in these simulation clustering results.

Experimental Discovery of a Predicted Octamer Conformation. One of the conformations produced by this simulation strategy, an octamer with one cis and seven trans amide bonds, was previously predicted by Voelz et al. to be the major conformer in solution,[26] but had never been experimentally characterized. During the course of this study, we obtained a crystal of peptoid octamer **Ncm8** (Chart 2). Upon solving the structure by single-crystal X-ray diffraction, we recognized the solid state structure as corresponding to this missing conformation.

Chart 2. Macrocycles Experimentally Characterized for Comparison to Simulation Results

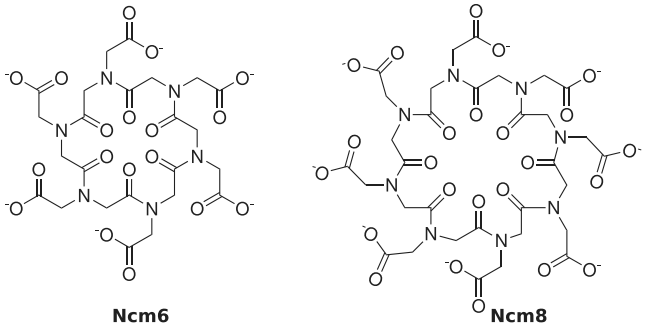

With the presence of rubidium cations as the counterions, compound **Ncm8** crystallized in the C12/c1 space group from aqueous solution. Viewed down the *a* axis of the crystal lattice as in Figure 3A, the **Ncm8** macrocycles stacked on each other in a tubular arrangement. Each tube formed by **Ncm8** with a backbone conformation of $Z_{Rc}Z_{St}Z_{Rt}Z_{St}Z_{Rt}Z_{St}Z_{Rt}Z_{Rt}$ interdigitated with the other tube stacked from the mirror imaged conformers showing the $Z_{Sc}Z_{Rt}Z_{St}Z_{Rt}Z_{St}Z_{Rt}Z_{St}Z_{St}$ conformation. Similarly, mirror-image conformations both bearing **ctttttttt** backbone amide patterns were observed in the simulation of cyclo-octasarcosine. Overlay of the 32 backbone heavy atoms between the crystal structure of **Ncm8** and the simulated **ctttttttt Sar8**, shown in Figure 3B, produced an RMSD value below 0.5 Å.

Correlated Motions. To identify concerted motions that might describe relationships between major conformations, we followed the hypothesis that the same motions would be evident across time scales in varying magnitude. We calculated covariance between all backbone dihedrals of all trajectories of each molecule (Figures 4, 5A,B, and S5−S8) as the square of the cyclic correlation coefficient.[43] This result shows a clear pattern of consecutive triplets of dihedrals exhibiting correlated motions: ϕ_i, ψ_i, ω_{i+1}. Since the ψ value never deviates far from 180°, these correlations define a crankshaft motion in peptoids as correlation of ϕ with the following ω. Additionally, some small correlations are found between nonadjacent ϕ dihedrals. These correlated motions can be observed in individual trajectories; a representative example is included as Figure S9.

Analysis of Plausible Transition Paths. To develop an understanding of possible transition paths between the conformations identified in this study, we performed simulations of the conversion between two hexamer conformations: those with **tttttt** and **ttcttc** amide patterns. These two simulation results correspond to two conformations discovered co-occupying a position within the unit cell of a recently published crystal structure of **Ncm6**.[24] The previously published crystal structures were determined at 100 K; to gain more insight into the thermodynamic properties of these unique conformational features and confirm their relevance under ambient conditions, we redetermined the crystal structures of compound **Ncm6** at 295 K in this work. No difference was observed in terms of the conformations adopted by compound **Ncm6** except the occupancy of the **ttcttc** conformer increased from 80% at 100 K to 84% at 295 K and the **tttttt** conformer decreased by the corresponding amount.

We used the Swarm-of-Trajectories string method[44] to study the transition pathway between the two corresponding conformations from the **Sar6** clustering results. In this method, an initial trajectory is established using Steered MD techniques, corresponding to a hypothetical transition pathway. This hypothetical path is divided into evenly spaced "images" (intermediate states along the path). For each of these images, the structure is constrained to the intermediate state and allowed to equilibrate, then freed from the constraints and allowed to relax. A large number ("swarm") of these trajectories are performed for each image, and their relaxed conformations are averaged to define the refined image. This refinement is repeated several times, with appropriate smoothing and recentering, until the simulation converges, and the resulting sequence of images defines the refined transition path. We initiated the simulation from several alternative plausible transition path hypotheses, clustered the resulting string of images using the previously described clustering strategy, and selected the pathway that, upon refinement, produced the smallest number of clusters along the transition path (see Table S2 for details). This result came from a simulation that steered first one amide inversion and then the opposing one, with all other degrees of freedom unconstrained. The refined pathway resulting from the Swarm-of-Trajectories simulation generally followed this initial steering but engaged several other amide bonds in the transition (see Figure S10). In accordance with the correlations observed during equilibrium simulations, the ϕ dihedral preceding each amide flips in concert with ω. The final transition path involves eight transition states, including two additional amide bonds briefly inverting.

https://doi.org/10.1021/acs.jpcb.2c01669
J. Phys. Chem. B 2022, 126, 5161−5174

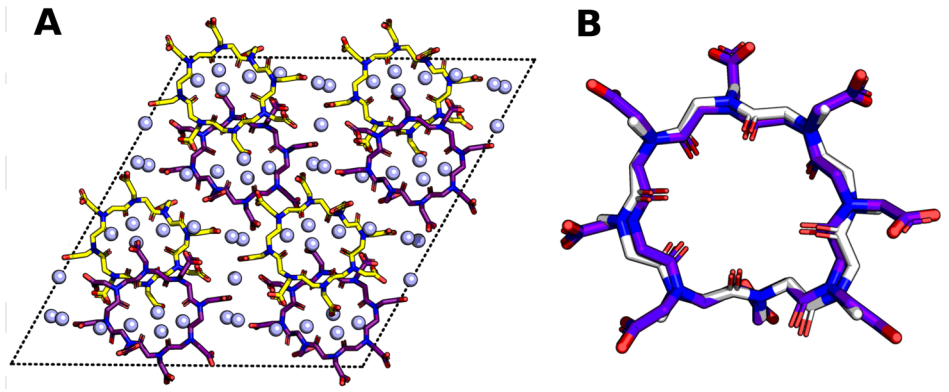

Figure 3. A novel **ctttttttt** octamer conformation predicted by this study and subsequently discovered in a crystal of **Ncm8** in complex with Rubidium (solvent not shown for clarity). (A) The unit cell contains eight molecules in two mirror-image conformations, depicted with carbon atoms in purple and yellow (viewed down the *a* direction). (B) The exemplar of the conformational cluster from the simulation of **Sar8** (white) matches the experimental structure of **Ncm8** (purple) to 0.4 Å RMSD, measured over all backbone atoms. Both mirror-image conformations were found in the simulation results; see SI for all models.

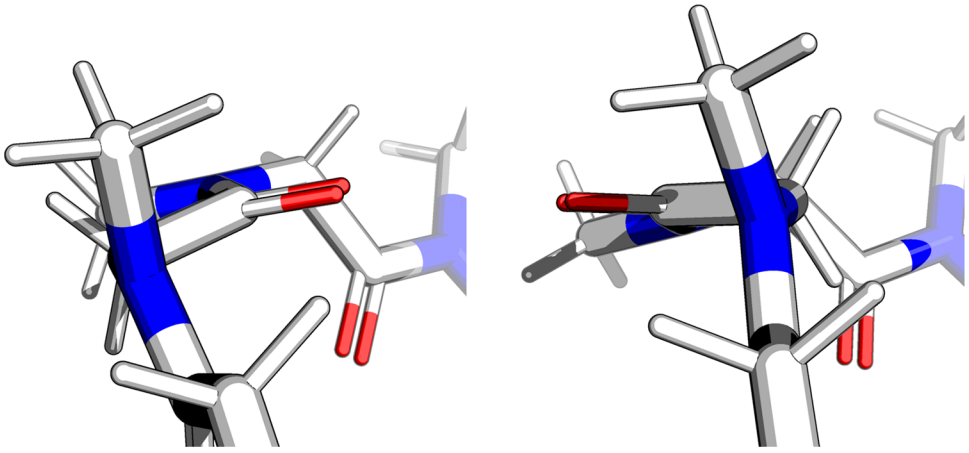

Figure 4. Peptoid Crankshaft Flip (viewed down ω).

DISCUSSION

The results of this study support two significant findings: first, we observe a reduction in ring strain as peptoid macrocycle size increases, allowing peptoid residues to preferentially populate the *Z* conformations; and second, we identify discrete ensembles of solution phase conformations for peptoid macrocycles. Moreover, we posit a crankshaft flip (by which amide isomerization is accommodated by inversion of the preceding ϕ dihedral), revealing these ensembles to be densely connected networks with clearly defined paths between conformations.

The sampling and clustering results reveal some additional, intriguing features of the conformational landscape of peptoid macrocycles. First, macrocycles of five to eight residues occupy a unique region of the size−flexibility spectrum. Tetramers are too small to be flexible, and nonamers are too large for all possible conformations to be easily enumerated. Second, macrocycles with even numbers of residues occupy simpler landscapes than those with odd numbers of residues.

Interpretation of this second observation is aided by reference to the geometric meaning of loop closure, which asserts, in part, that all bond vectors must sum to zero, and all dihedral angles must also sum to zero. The peptoid *Z* conformations yield N−N residue vectors of two different lengths (≈ 2.9 Å for **c**, ≈3.7 Å for **t**) and dihedral angles between consecutive amide planes near ±90°. Since even numbers of right angles sum to 0° or 180°, cyclic peptoids of even numbers of residues are broadly compatible with *Z*. Odd numbered macrocycles exhibit ring strain, which may be evident in residues slightly distorted from the ideal *Z* conformation or in a single residue adopting a higher-energy alternative conformation.

Sampling and Clustering. The set of conformations produced by this sampling and clustering strategy proved to be smaller than the number of seeds in half of the molecules studied (see Table 3), and dramatically smaller than any measure of the total number of conformations that could be populated by linear analogues of the same molecules. For example, combinatorially sampling the four *Z* conformations in a linear hexamer would yield $4^6 = 4096$ conformations; taking into account the equivalence of cyclic permutations reduces this number to 700 (see SI eq 1), while only 22 are populated in this study. This limited number of populated conformations demonstrates and quantifies the dramatic impact of the conformational constraint imposed by cyclization, and indicates that the conformational ensembles presented here are not inappropriately complex. Since the seeds were generated to populate all amide bond patterns, this was already a limited set of hypothetical conformations; the MD simulations eliminated some of these.

https://doi.org/10.1021/acs.jpcb.2c01669
J. Phys. Chem. B 2022, 126, 5161−5174

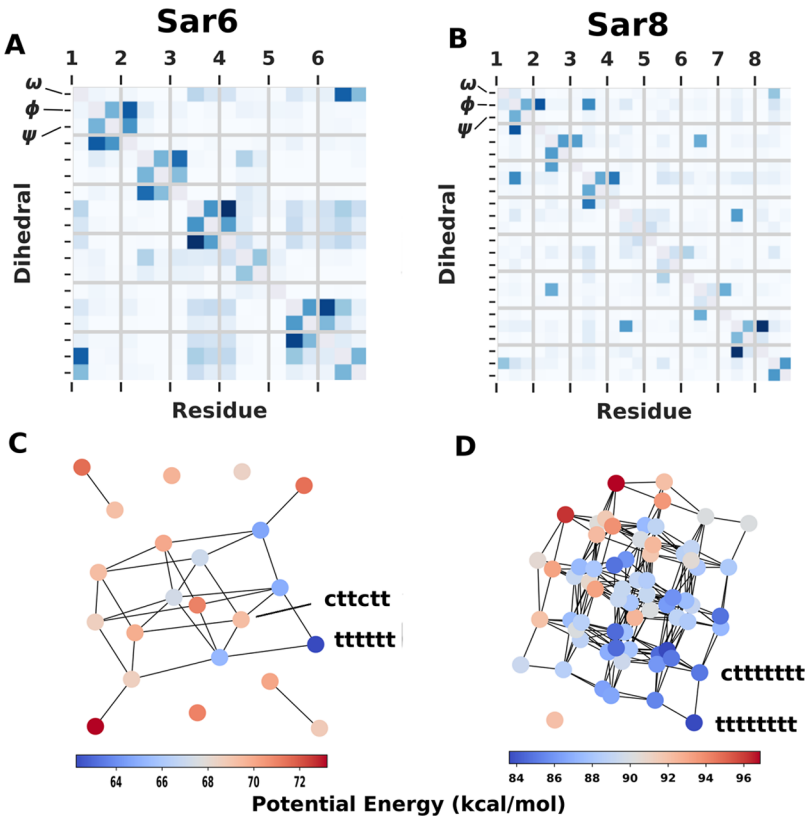

Figure 5. (A,B) Circular covariance calculated between all dihedrals in **Sar6** (A), **Sar8** (B) over all simulations. (C,D) Network visualization of conformational clusters connected by "crankshaft flips" in **Sar6** (C), **Sar8** (D). Nodes are colored by single-point GAFF energy calculation, a measure of conformational potential energy (low energy in blue). Conformations discussed in regard to experimental structures **Ncm6**, **Ncm8** are labeled with amide pattern.

Table 3. Comparison between Sampled Conformations ("Seeds") and Observed Conformations ("Clusters")

cycle size	# seeds	# clusters
4	12	21
5	16	14
6	28	22
7	40	74
8	72	68
9	120	163

Although the sampling and clustering strategy treated **Sar4** inadequately (vide supra), generating far too many conformations of a molecule understood to be rigid, these results are illustrative of a broader trend over all the macrocycles simulated, evident in Figure 2B,C: As macrocycle size increases, the peptoid residues relax toward the Z conformations. On the basis of this observation, **Sar5**, **Sar6**, **Sar7**, and **Sar8** appear to occupy a privileged zone between highly rigid and highly flexible structures.

Heptamer. The heptamer populates notably more conformations than either the hexamer or the octamer. As in the pentamer, many of the populated heptamer conformations (including the global minimum) contain one residue in a $C_{7\beta}$ conformation. The sole experimentally determined peptoid heptamer structure features six residues in Z conformations and one in $C_{7\beta}$, and the conformation predicted by this simulation to be the lowest in energy matches the experimental structure quite closely, as shown in Table 2.

Nonamer. The failure to reproduce the lone relevant experimental structure of a peptoid cyclononamer (vide supra) demonstrates the incompleteness of the large set of conformational clusters found for this molecule. The absence of any dominant cluster, along with the large number of clusters and the diminished correlations between dihedral angles (Figure S8), implies that cyclic peptoids of nine residues behave much more like unconstrained oligomers than do the smaller macrocycles. The results also indicate that octamers may be the upper size limit of peptoid macrocycle for which our approach can be considered comprehensive.

Comparison to Experimental Results. The success of this study in reproducing all relevant experimental structures between five and eight residues to a high degree of accuracy indicates that the conformational ensembles presented here are not inappropriately simple for this size range. In particular, the successful prediction of the **Sar5** and **Sar7** solid state conformations, with their distinctive $C_{7\beta}$ residues, vindicates the decision not to sample this region of dihedral space explicitly, but to rely upon the Molecular Dynamics simulations to identify local minima.

Three macrocycle structures composed of alternating N-substituted glycine residues with Proline (or a derivative) have been solved that adopt conformations not observed in these results.[68−70] These omissions in the simulation results demonstrate that some high energy conformations may be adopted by highly constrained macrocycles; in fact, Proline positioning is a well-developed design principle for stabilizing peptide macrocycles in diverse conformations.[31]

https://doi.org/10.1021/acs.jpcb.2c01669
J. Phys. Chem. B 2022, 126, 5161−5174

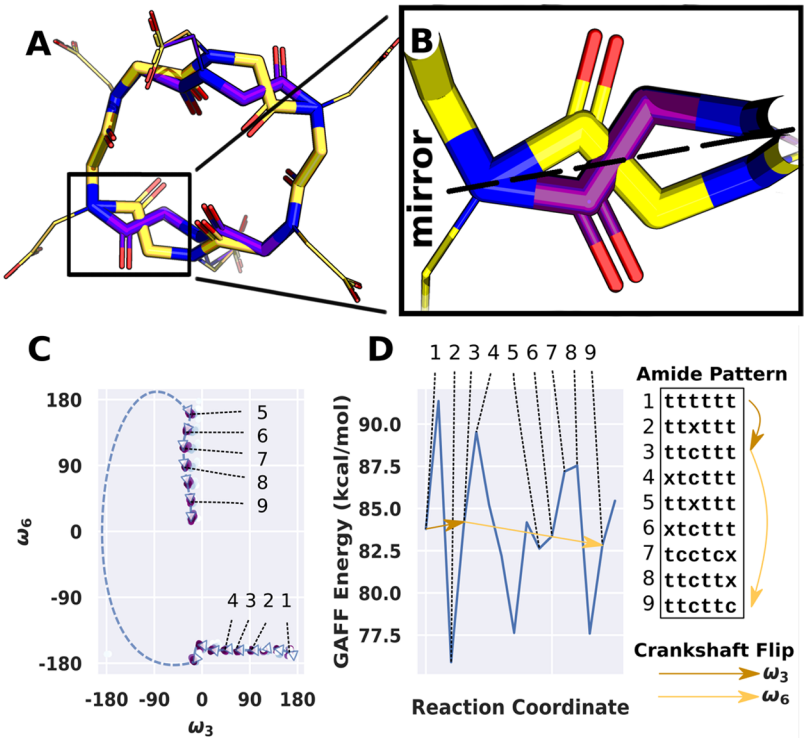

Figure 6. (A B) One site from the X-ray crystal structure of **Ncm6** gathered at 295 K. One of two sites in the unit cell is variably occupied by two distinct conformations. The major conformer (82% occupancy) has a **cttctt** amide pattern, while the minor conformer is identical to the other conformation found in the unit cell, with a **tttttt** amide pattern. The relationship between these two structures can be understood as two symmetric crankshaft flips, as the ϕ and ψ dihedrals preceding the inverting ω dihedral are approximately mirrored between the two conformations (ϕ_1 = 84.5°, ψ_1 = −169.3°, ω_1 = 3.64°), (ϕ_2 = −75.1°, ψ_2 = 169.1°, ω_2 = 176.9°). (C) Pathway describing the transition shown in A, simulated using Steered MD and refined using Swarm-of-Trajectories string method. CV 1 and CV 2 are the torsions corresponding to ω_3 and ω_6, steered from 180° to 0°. (D) Potential energy profile along the transition path shown in C. (C,D) Transitions between conformational clusters (as defined in the text) are annotated 1−9.

Discovery of Novel Octamer Structure. Previous REMD (replica exchange molecular dynamics) work from Voelz et al. showed that conformations of cyclo-octasarcosine with **ctttttt** and **ttttttt** backbone amide patterns are the lowest free energy states in solution, with a free energy difference less than 0.3 kcal/mol.[26] The conformational difference between these two states can be viewed as the outcome of an individual crankshaft flip. The landscape of **Sar8** mapped in the present work agrees with the calculated free energy difference[26] (Figure 5D). In addition, although cyclo-octasarcosine and several other cyclo-octamer peptoids adopt a backbone conformation with a **ccttcctt** amide pattern in the crystal lattice,[71] we experimentally observed that cyclo-octa(*N*-carboxymethyl)glycine (**Ncm8**) adopted a backbone conformation with the **ctttttt** amide pattern (Figure 3). This discovery realizes a prediction from the theoretical treatment of peptoid macrocycles established in this work. In addition, the **ctttttt** octamer crystal structure presented here is also a rare example of an oligomer with a high degree of sequence symmetry crystallizing in a space group with no point group symmetry (other than an inversion center relating the two planar enantiomers). Such low-symmetry conformations are expected to dominate in the solution phase,[26] and are therefore of great interest to designers of bioactive macrocycles.

Correlated Motion. The observed local dihedral correlations match a pattern known in theoretical studies of polymer conformations as a "crankshaft motion",[36] which results in the repositioning of two adjacent backbone atoms with minimal perturbation of the flanking chain. The conformational change is illustrated using 3D models in Figure 4. The motion of ψ is worth noting because, while correlated with ϕ and ω, it is small in magnitude and does not involve a transition between bins in this dimension. In peptides, an analogous crankshaft motion, anticorrelation between ψ_{i-1} and ϕ_i, has been invoked to explain NMR relaxation order parameters,[39,72] and the corresponding crankshaft flip has been observed in simulations of linear peptides[39] as well as in crystal structures of antibody loops,[37] and has been applied to enhance sampling of cyclic peptides in Metadynamics simulations.[38]

Significance of the Crankshaft Flip. The hypothesis that the crankshaft motion observed in these simulations also allows for a flip suggests a straightforward interconversion pathway between similar conformations in all but the smallest macrocycles: an isomerization of one amide bond in conjunction with an inversion of the preceding two bond dihedrals. This concerted motion is the peptoid equivalent of the crankshaft flip observed in peptide loops: in peptides, the amide bond remains rigid while the flanking ϕ and ψ dihedrals flip. The result of either such flip is to redirect the amide carbonyl (and thus the dipole moment) while minimally perturbing any side chains.

The descriptive power of these crankshaft flips in cyclic peptoid conformations is apparent in a recently published crystal structure of a cyclohexamer,[24] re-examined in this study. The unit cell contains two distinct sites: one is occupied by the high-symmetry, metal-coordinating, all trans conformation; the other site is partially occupied by the same conformation, but the major occupant is a newly observed **cttctt** conformation

https://doi.org/10.1021/acs.jpcb.2c01669
J. Phys. Chem. B 2022, 126, 5161−5174

(Figure 6A). These two conformations are related by two crankshaft flips on opposite residues. In accordance with the theory presented here, the residues preceding the two *cis*-amide bonds are mirrored relative to their counterpart in the minor conformer (Figure 6B). The amide carbonyls flip out, diminishing the coordination of the central metal ion from octahedral to trigonal bipyramidal, without perturbing the side chains, which in this structure are playing a distinct metal-coordinating role. The crankshaft flip furnishes a clear description of the conformational changes behind this result.

Network Interpretation of the Cyclic Peptoid Conformational Landscape. Although the crankshaft flip may not always be the Minimum Free Energy Path between two related conformations, its descriptive power suggests a novel view of the energy landscape for each macrocycle: as a network of conformations (nodes) connected by single crankshaft flips (links).

The networks for all macrocycles larger than the pentamer show a high degree of interconnectedness, appearing as a large "continent" and small "islands" (Figures 5C,D and S11−S14). The islands in the network consist of any conformational cluster containing one residue out of the *Z* bin, which cannot be accessed purely through these moves. These clusters are insignificant in the hexamer and octamer. The heptamer shows two disconnected continents (see Figure S12), illustrating how enantiomeric pairs arise from the planar chirality of the amide bonds, as De Riccardis, D'Amato et al. have elucidated.[18,25] These enantiomeric conformation families disappear in the even-numbered macrocycles as a result of their symmetry: the highest-symmetry conformation in each is the all *trans*-amide, which is comprised of alternating positive, negative ϕ values for a repeat unit of two residues. In the case of homo-oligomer macrocycles exclusively, a cyclic permutation of the pattern by one residue leads to an equivalent form.

Analysis of Plausible Transition Paths. Mapping the interconversion pathway between the two backbone conformations (**ttttt**, **cttctt**) of **Sar6** using the Swarm-of-Trajectories String Method[44] reveals a pathway far more complex than two consecutive crankshaft flips. The first flip is straightforward, but the structure then passes through several intermediates on the way to the second flip, including two amide bonds isomerizing to cis and back to trans in the final structure (Figure 6). The free energy barrier to interconversion between these two conformations is very large, and it would require significant sampling enhancement to find this alternative conformation in an uninformed MD study. Guided by the crankshaft flip, only two moves are required to find the target, each move guiding the molecule into an adjacent energy well. The crankshaft flip greatly simplifies the description (and accelerates the sampling) of conformational conversions in peptoid macrocycles.

CONCLUSIONS

Recent insights simplifying the conformational landscape of peptoid residues offered hope that the landscape of cyclic peptoids[20] could be mapped, and here we have provided an overview of many of the interesting valleys. The landscapes of cyclohexamers and cyclo-octamers, in particular, now appear to be mapped almost completely. The recent publication of novel conformations of hexamers[24] and octamers[23] has invigorated the field; the map of conformations connected by crankshaft flips should guide peptoid explorers to the more challenging, hidden valleys of low-symmetry conformations, the first example of which we have now demonstrated experimentally. Proper side chain selection will facilitate stabilization of specific conformations, enabling design of peptoid macromolecules with exceptional precision. Further exploration may require the determination of additional solution structure by NMR, but the peptoid chemist's toolbox is well-equipped for this task too: a variety of peptoid side chains have been well-established to provide good peak dispersion by NMR. The complex sequences required to stabilize and functionalize such structures will also facilitate NMR peak assignment.

The related crankshaft flip in cyclic peptides has been used to develop collective variables for MetaDynamics sampling,[35] and the concerted motion described here could be used for an analogous purpose in peptoids. In particular, it could be a useful guide to the conformational sampling of even larger macrocycles, where only the barest exploration has been made,[27,73] and also in Monte Carlo techniques, where crankshaft flips were first identified. Crankshaft flips, or smaller crankshaft motions, could also be employed to diversify linear peptoid backbone conformations during modeling and design tasks, as they reduce the lever-arm effects that are induced when sampling individual backbone dihedral angles, functioning in a similar way to the "shear" motions[74] used to sample peptide and protein conformations. As the field of structured peptoid design expands, these insights will enable design of peptoid loops that connect structural motifs within protein-mimetic foldamers.

A growing body of literature is focused on the dynamics of cyclic peptides, and not only on stabilizing a single conformation. The conformations and dynamics presented here will advance analogous studies of cyclic peptoids. It remains to be discovered whether the crankshaft flip described here corresponds to a realistic chemical transition pathway, or is merely a theoretical geometric shortcut. The answer to this question could inspire exciting designs for multistate, switchable macrocycles. The conformational ensembles identified here, and provided in the SI, strengthen the foundation of our ongoing efforts to design bioactive peptoid macrocycles.

ASSOCIATED CONTENT

Supporting Information

The Supporting Information is available free of charge at https://pubs.acs.org/doi/10.1021/acs.jpcb.2c01669.

Additional details on experimental and computational methods; analytical data for Ncm6, Ncm8, sampling, covariance, and network analysis for Sar4, Sar5, Sar7, and Sar9 (PDF)

Archive of cluster exemplars (in PDB format) for all clusters identified (ZIP)

Crystal structure files for Ncm6 (ZIP)

Crystal structure files for Ncm8 (ZIP)

AUTHOR INFORMATION

Corresponding Authors

Kent Kirshenbaum − *Department of Chemistry, New York University, New York, New York 10003, United States*; Phone: 212-998-8486; Email: kent@nyu.edu

P. Douglas Renfrew − *Center for Computational Biology, Flatiron Institute, New York, New York 10010, United States*; Phone: 646-603-3717; Email: pdrenfrew@flatironinstitute.org

https://doi.org/10.1021/acs.jpcb.2c01669
J. Phys. Chem. B 2022, 126, 5161−5174

Authors

James R. B. Eastwood − *Department of Chemistry, New York University, New York, New York 10003, United States;* orcid.org/0000-0003-3895-5227

Linhai Jiang − *Department of Chemistry, New York University, New York, New York 10003, United States;* orcid.org/0000-0002-9403-9170

Richard Bonneau − *Center for Data Science, New York University, New York, New York 10011, United States; Center for Computational Biology, Flatiron Institute, New York, New York 10010, United States*

Complete contact information is available at: https://pubs.acs.org/10.1021/acs.jpcb.2c01669

Notes

The authors declare no competing financial interest.

■ ACKNOWLEDGMENTS

This study was supported by award CHE-2002890 from the National Science Foundation (NSF). The authors thank the Flatiron Institute Scientific Computing Core for providing support for the extensive computational resources required to complete this research. The authors thank Dr. Trinanjana Mandal for the assistance on electron dispersive spectroscopy and Dr. Chunhua Tony Hu for determining the X-ray crystal structures of **Ncm6** and **Ncm8**. The authors acknowledge the contribution of the X-ray facility at NYU's Materials Research Science and Engineering Center (MRSEC) program under NSF Awards DMR-0820341 and DMR-1420073. L.J. gratefully acknowledges the New York University Chemistry Department for the Margaret and Herman Sokol Fellowship.

■ REFERENCES

(1) Schneider, J. A.; Craven, T. W.; Kasper, A. C.; Yun, C.; Haugbro, M.; Briggs, E. M.; Svetlov, V.; Nudler, E.; Knaut, H.; Bonneau, R.; Garabedian, M. J.; Kirshenbaum, K.; Logan, S. K.; et al. Design of Peptoid-Peptide Macrocycles to Inhibit the β-catenin TCF Interaction in Prostate Cancer. *Nat. Commun.* **2018**, *9*, 4396.

(2) Mulligan, V. K.; Workman, S.; Sun, T.; Rettie, S.; Li, X.; Worrall, L. J.; Craven, T. W.; King, D. T.; Hosseinzadeh, P.; Watkins, A. M.; Renfrew, P. D.; Guffy, S.; Labonte, J. W.; Moretti, R.; Bonneau, R.; Strynadka, N. C. J.; Baker, D. Computationally Designed Peptide Macrocycle Inhibitors of New Delhi Metallo-β-lactamase 1. *Proc. Natl. Acad. Sci. U.S.A.* **2021**, *118* (12), e2012800118.

(3) Johansen-Leete, J.; Ullrich, S.; Fry, S. E.; Frkic, R.; Bedding, M. J.; Aggarwal, A.; Ashhurst, A. S.; Ekanayake, K. B.; Mahawaththa, M. C.; Sasi, V. M.; et al. Antiviral cyclic peptides targeting the main protease of SARS-CoV-2. *Chem. Sci.* **2022**, *13*, 3826−3836.

(4) Shin, M. K.; Hyun, Y. J.; Lee, J. H.; Lim, H. S. Comparison of Cell Permeability of Cyclic Peptoids and Linear Peptoids. *ACS Comb. Sci.* **2018**, *20*, 237−242.

(5) Shin, S. B. Y.; Yoo, B.; Todaro, L. J.; Kirshenbaum, K. Cyclic Peptoids. *J. Am. Chem. Soc.* **2007**, *129*, 3218−3225.

(6) Webster, A. M.; Cobb, S. L. Recent Advances in the Synthesis of Peptoid Macrocycles. *Chemistry, A European Journal* **2018**, *24*, 7560−7573.

(7) D'Amato, A.; Volpe, R.; Vaccaro, M. C.; Terracciano, S.; Bruno, I.; Tosolini, M.; Tedesco, C.; Pierri, G.; Tecilla, P.; Costabile, C.; et al. Cyclic Peptoids as Mycotoxin Mimics: An Exploration of Their Structural and Biological Properties. *J. Org. Chem.* **2017**, *82*, 8848−8863.

(8) Bonnet, P.; Agrafiotis, D. K.; Zhu, F.; Martin, E. Conformational Analysis of Macrocycles: Finding What Common Search Methods Miss. *J. Chem. Inf. Model.* **2009**, *49*, 2242−2259.

(9) Labute, P. LowModeMD - Implicit Low-Mode Velocity Filtering Applied to Conformational Search of Macrocycles and Protein Loops. *J. Chem. Inf. Model.* **2010**, *50*, 792−800.

(10) Watts, K. S.; Dalal, P.; Tebben, A. J.; Cheney, D. L.; Shelley, J. C. Macrocycle Conformational Sampling with Macromodel. *J. Chem. Inf. Model.* **2014**, *54*, 2680−2696.

(11) Coutsias, E. A.; Lexa, K. W.; Wester, M. J.; Pollock, S. N.; Jacobson, M. P. Exhaustive Conformational Sampling of Complex Fused Ring Macrocycles Using Inverse Kinematics. *J. Chem. Theory Comput.* **2016**, *12*, 4674−4687.

(12) Gutten, O.; Bím, D.; Řezáč, J.; Rulíšek, L. Macrocycle Conformational Sampling by DFT-D3/COSMO-RS Methodology. *J. Chem. Inf. Model.* **2018**, *58*, 48−60.

(13) Sindhikara, D.; Spronk, S. A.; Day, T.; Borrelli, K.; Cheney, D. L.; Posy, S. L. Improving Accuracy, Diversity, and Speed with Prime Macrocycle Conformational Sampling. *J. Chem. Inf. Model.* **2017**, *57*, 1881−1894.

(14) Fuchs, J. E.; Kamenik, A. S.; Lessel, U.; Liedl, K. R.; Fox, T. Peptidic Macrocycles - Conformational Sampling and Thermodynamic Characterization. *J. Chem. Inf. Model.* **2018**, *58*, 982−992.

(15) Jain, A. N.; Cleves, A. E.; Gao, Q.; Wang, X.; Liu, Y.; Sherer, E. C.; Reibarkh, M. Y. Complex Macrocycle Exploration: Parallel, Heuristic, and Constraint-Based Conformer Generation using ForceGen. *Journal of Computer-Aided Molecular Design* **2019**, *33*, 531−558.

(16) Wang, S.; Witek, J.; Landrum, G. A.; Riniker, S. Improving Conformer Generation for Small Rings and Macrocycles Based on Distance Geometry and Experimental Torsional-Angle Preferences. *J. Chem. Inf. Model.* **2020**, *60*, 2044−2058.

(17) Alogheli, H.; Olanders, G.; Schaal, W.; Brandt, P.; Karlén, A. Docking of Macrocycles: Comparing Rigid and Flexible Docking in Glide. *J. Chem. Inf. Model.* **2017**, *57*, 190−202.

(18) D'Amato, A.; Schettini, R.; Della Sala, G.; Costabile, C.; Tedesco, C.; Izzo, I.; De Riccardis, F. Conformational Isomerism in Cyclic Peptoids and Its Specification. *Organic & Biomolecular Chemistry* **2017**, *15*, 9932−9942.

(19) Sui, Q.; Borchardt, D.; Rabenstein, D. L. Kinetics and Equilibria of cis/trans Isomerization of Backbone Amide Bonds in Peptoids. *J. Am. Chem. Soc.* **2007**, *129*, 12042−12048.

(20) Spencer, R. K.; Butterfoss, G. L.; Edison, J. R.; Eastwood, J. R.; Whitelam, S.; Kirshenbaum, K.; Zuckermann, R. N. Stereochemistry of Polypeptoid Chain Configurations. *Biopolymers* **2019**, *110*, e23266.

(21) Dale, J.; Titlestad, K. Cyclic Oligopeptides of Sarcosine (N-methylglycine). *Journal of the Chemical Society D: Chemical Communications* **1969**, 656.

(22) De Cola, C.; Ianniello, G.; Tedesco, C.; Erra, L.; Vaughan, G.; Izzo, I.; Nardone, B.; De Riccardis, F. Structural Effects of Proline Substitution and Metal Binding on Hexameric Cyclic Peptoids. *Org. Lett.* **2013**, *15*, 598−601.

(23) D'Amato, A.; Pierri, G.; Tedesco, C.; Della Sala, G.; Izzo, I.; Costabile, C.; De Riccardis, F. Reverse Turn and Loop Secondary Structures in Stereodefined Cyclic Peptoid Scaffolds. *Journal of Organic Chemistry* **2019**, *84*, 10911−10928.

(24) Jiang, L.; Hu, C. T.; De Riccardis, F.; Kirshenbaum, K. Elaborate Supramolecular Architectures Formed by Co-Assembly of Metal Species and Peptoid Macrocycles. *Cryst. Growth Des.* **2021**, *21*, 3889−3901.

(25) De Riccardis, F. The Challenge of Conformational Isomerism in Cyclic Peptoids. *Eur. J. Org. Chem.* **2020**, *2020*, 2981−2994.

(26) Voelz, V. A.; Dill, K. A.; Chorny, I. Peptoid Conformational Free Energy Landscapes from Implicit-Solvent Molecular Simulations in AMBER. *Biopolymers* **2011**, *96*, 639−650.

(27) Butterfoss, G. L.; Yoo, B.; Jaworski, J. N.; Chorny, I.; Dill, K. A.; Zuckermann, R. N.; Bonneau, R.; Kirshenbaum, K.; Voelz, V. A. De novo Structure Prediction and Experimental Characterization of Folded Peptoid Oligomers. *Proc. Natl. Acad. Sci. U. S. A.* **2012**, *109*, 14320−14325.

(28) Yu, H.; Lin, Y. S. Toward Structure Prediction of Cyclic Peptides. *Phys. Chem. Chem. Phys.* **2015**, *17*, 4210−4219.

(29) Nguyen, Q. N. N.; Schwochert, J.; Tantillo, D. J.; Lokey, R. S. Using 1H and 13C NMR Chemical Shifts to Determine Cyclic Peptide Conformations: A Combined Molecular Dynamics and Quantum Mechanics Approach. *Phys. Chem. Chem. Phys.* **2018**, *20*, 14003−14012.
(30) Hurley, M. F. D.; Northrup, J. D.; Ge, Y.; Schafmeister, C. E.; Voelz, V. A. Metal Cation-Binding Mechanisms of Q-Proline Peptoid Macrocycles in Solution. *J. Chem. Inf. Model* **2021**, *61* (6), 2818−2828.
(31) Hosseinzadeh, P.; Bhardwaj, G.; Mulligan, V. K.; Shortridge, M. D.; Craven, T. W.; Pardo-Avila, F.; Rettie, S. A.; Kim, D. E.; Silva, D.-A. A.; Ibrahim, Y. M.; et al. Comprehensive Computational Design of Ordered Peptide Macrocycles. *Science* **2017**, *358*, 1461−1466.
(32) Warvari, H. E.; Knaell, K. K.; Scott, R. A. Monte Carlo Calculations on Polypeptide Chains. IV. Hard-Sphere Models for Randomly Coiling Polysarcosine and Poly- *N* -Methyl-L-Alanine. *J. Chem. Phys.* **1972**, *56*, 2903−2911.
(33) Sisido, M.; Imanishi, Y.; Higashimura, T. Monte Carlo Calculation on trans/cis-Polysarcosine. *Macromolecules* **1976**, *9*, 389−395.
(34) Butterfoss, G. L.; Renfrew, P. D.; Kuhlman, B.; Kirshenbaum, K.; Bonneau, R. A Preliminary Survey of the Peptoid Folding Landscape. *J. Am. Chem. Soc.* **2009**, *131*, 16798−16807.
(35) McHugh, S. M.; Rogers, J. R.; Yu, H.; Lin, Y.-S. Insights into How Cyclic Peptides Switch Conformations. *J. Chem. Theory Comput.* **2016**, *12*, 2480−2488.
(36) Hilhorst, H. J.; Deutch, J. M. Analysis of Monte Carlo Results on the Kinetics of Lattice Polymer Chains with Excluded Volume. *J. Chem. Phys.* **1975**, *63*, 5153−5161.
(37) North, B.; Lehmann, A.; Dunbrack, R. L. A New Clustering of Antibody CDR Loop Conformations. *J. Mol. Biol.* **2011**, *406*, 228−256.
(38) Damjanovic, J.; Miao, J.; Huang, H.; Lin, Y.-S. Elucidating Solution Structures of Cyclic Peptides Using Molecular Dynamics Simulations. *Chem. Rev.* **2021**, *121*, 2292−2324.
(39) Fadel, A. R.; Jin, D. Q.; Montelione, G. T.; Levy, R. M. Crankshaft Motions of the Polypeptide Backbone in Molecular Dynamics Simulations of Human Type-α; Transforming Growth Factor. *Journal of Biomolecular NMR* **1995**, *6*, 221−226.
(40) Alford, R. F.; Leaver-Fay, A.; Jeliazkov, J. R.; O'Meara, M. J.; DiMaio, F. P.; Park, H.; Shapovalov, M. V.; Renfrew, P. D.; Mulligan, V. K.; Kappel, K.; et al. The Rosetta All-Atom Energy Function for Macromolecular Modeling and Design. *J. Chem. Theory Comput.* **2017**, *13*, 3031−3048.
(41) Frisch, M. J.; Trucks, G. W.; Schlegel, H. B.; Scuseria, G. E.; Robb, M. A.; Cheeseman, J. R.; Scalmani, G.; Barone, V.; Mennucci, B.; Petersson, G. A.; Nakatsuji, H.; Caricato, M.; Li, X.; Hratchian, H. P.; Izmaylov, A. F.; Bloino, J.; Zheng, G.; Sonnenberg, J. L.; Hada, M.; Ehara, M.; Toyota, K.; Fukuda, R.; Hasegawa, J.; Ishida, M.; Nakajima, T.; Honda, Y.; Kitao, O.; Nakai, H.; Vreven, T.; Montgomery, J. A., Jr.; Peralta, J. E.; Ogliaro, F.; Bearpark, M.; Heyd, J. J.; Brothers, E.; Kudin, K. N.; Staroverov, V. N.; Kobayashi, R.; Normand, J.; Raghavachari, K.; Rendell, A.; Burant, J. C.; Iyengar, S. S.; Tomasi, J.; Cossi, M.; Rega, N.; Millam, J. M.; Klene, M.; Knox, J. E.; Cross, J. B.; Bakken, V.; Adamo, C.; Jaramillo, J.; Gomperts, R.; Stratmann, R. E.; Yazyev, O.; Austin, A. J.; Cammi, R.; Pomelli, C.; Ochterski, J. W.; Martin, R. L.; Morokuma, K.; Zakrzewski, V. G.; Voth, G. A.; Salvador, P.; Dannenberg, J. J.; Dapprich, S.; Daniels, A. D.; Farkas, O.; Foresman, J. B.; Ortiz, J. V.; Cioslowski, J.; Fox, D. J. *Gaussian 09*, revision E.01; Gaussian, Inc.: Wallingford, CT, 2009.
(42) Wang, J.; Wolf, R. M.; Caldwell, J. W.; Kollman, P. A.; Case, D. A. Development and Testing of a General Amber Force Field. *J. Comput. Chem.* **2004**, *25*, 1157−1174.
(43) Jammalamadaka, S. R. *Topics in Circular Statistics; Series on Multivariate Analysis*; World Scientific Publishing Company: Singapore, 2001; Vol. *5*.
(44) Pan, A. C.; Sezer, D.; Roux, B. Finding Transition Pathways Using the String Method with Swarms of Trajectories. *J. Phys. Chem. B* **2008**, *112*, 3432−3440.
(45) Case, D.; Ben-Shalom, I.; Brozell, S.; Cerutti, D.; Cheatham, T.; Cruzeiro, V.; Darden, T.; Duke, R.; Ghoreshi, M.; Gilson, M. et al. *AMBER 2018*; University of California: San Francisco, CA, 2018.
(46) Dale, J.; Groth, P.; Titlestad, K.; Enzell, C. R.; Christensen, A.; Schroll, G. Preferred Conformational Angles in Peptides Unperturbed by Hydrogen Bonding and α-Substituents. *Acta Chem. Scand.* **1977**, *31b*, 523−526.
(47) Head-Gordon, T.; Head-Gordon, M.; Frisch, M. J.; Brooks, C. L.; Pople, J. A. Theoretical Study of Blocked Glycine and Alanine Peptide Analogs. *J. Am. Chem. Soc.* **1991**, *113*, 5989−5997.
(48) Moehle, K.; Hofmann, H.-J. Peptides and Peptoids—A Quantum Chemical Structure Comparison. *Biopolymers* **1996**, *38*, 781−790.
(49) Groth, P.; Ronnquist, O.; Aarskog, J.; Nielsen, P. H.; Rasmussen, S. E.; Sunde, E.; Sørensen, N. A. Crystal Structure of Cyclotetrasarcosyl. *Acta Chem. Scand.* **1970**, *24*, 780−790.
(50) Titlestad, K.; Groth, P.; Dale, J. Crystal and Solution Conformation of Cyclopentasarcosyl. *J. Chem. Soc., Chem. Commun.* **1973**, 646−647.
(51) Groth, P.; Esperas, S.; Husebye, S.; Mikalsen, Øy.; Southern, J. T.; Edlund, K.; Eliasen, M.; Herskind, C.; Laursen, T.; Pedersen, P. M. Crystal Structure of Cycloheptasarcosyl Hydrate. *Acta Chem. Scand.* **1975**, *29a*, 38−44.
(52) Groth, P.; Søtofte, I.; Koskinen, R.; Pohjonen, M.-L.; Koskikallio, J. Crystal Conformation of Cyclotrisarcosyl at −160 °C. *Acta Chem. Scand.* **1976**, *30a*, 838−840.
(53) Culf, A. S.; Čuperlović Culf, M.; Léger, D. A.; Decken, A. Small Head-to-Tail Macrocyclic α-Peptoids. *Org. Lett.* **2014**, *16*, 2780−2783.
(54) Dale, J.; Titlestad, K.; Hornfeldt, A.-B.; Liaaen-Jensen, S.; Schroll, G.; Altona, C. Conformational Processes in Simple Cyclic Peptides. *Acta Chem. Scand.* **1975**, *29b*, 353−361.
(55) Onufriev, A.; Bashford, D.; Case, D. A. Exploring Protein Native States and Large-Scale Conformational Changes with a Modified Generalized Born Model. *Proteins: Struct., Funct., Bioinf.* **2004**, *55*, 383−394.
(56) Maulucci, N.; Izzo, I.; Bifulco, G.; Aliberti, A.; De Cola, C.; Comegna, D.; Gaeta, C.; Napolitano, A.; Pizza, C.; Tedesco, C.; et al. Synthesis, Structures, and Properties of Nine-, Twelve-, and Eighteen-Membered N-Benzyloxyethyl Cyclic α-Peptoids. *Chem. Commun.* **2008**, 3927−3929.
(57) Tedesco, C.; Erra, L.; Izzo, I.; De Riccardis, F. Solid State Assembly of Cyclic α-Peptoids. *CrystEngComm* **2014**, *16*, 3667−3687.
(58) Groth, P.; Thorstenson, T.; Nasakkala, E.; Kjekshus, A.; Rakke, T.; Andresen, A. F. Crystal Conformation of Cyclohexasarcosyl $2CH_3OH$ at − 156°C. *Acta Chem. Scand.* **1977**, *31a*, 232−234.
(59) Shah, N. H.; Butterfoss, G. L.; Nguyen, K.; Yoo, B.; Bonneau, R.; Rabenstein, D. L.; Kirshenbaum, K. Oligo(N-aryl glycines): A New Twist on Structured Peptoids. *J. Am. Chem. Soc.* **2008**, *130*, 16622−16632.
(60) Paul, B.; Butterfoss, G. L.; Boswell, M. G.; Huang, M. L.; Bonneau, R.; Wolf, C.; Kirshenbaum, K. N-Naphthyl Peptoid Foldamers Exhibiting Atropisomerism. *Org. Lett.* **2012**, *14*, 926−929.
(61) Tedesco, C.; Macedi, E.; Meli, A.; Pierri, G.; Sala, G. D.; Drathen, C.; Fitch, A. N.; Vaughan, G. B. M.; Izzo, I.; De Riccardis, F. Synthesis, Crystallization, X-ray Structural Characterization and Solid-State Assembly of a Cyclic Hexapeptoid with Propargyl and Methoxyethyl Side Chains. *Acta Crystallogr.* **2017**, *B73*, 399−412.
(62) Pierri, G.; Schettini, R.; Nuss, J.; Dinnebier, R. E.; De Riccardis, F.; Izzo, I.; Tedesco, C. Cyclic Hexapeptoids with N-Alkyl Side Chains: Solid-State Assembly and Thermal Behaviour. *CrystEngComm* **2020**, *22*, 6371−6384.
(63) Schettini, R.; Tosolini, M.; ur Rehman, J.; Shah, M. R.; Pierri, G.; Tedesco, C.; Della Sala, G.; De Riccardis, F.; Tecilla, P.; Izzo, I. Role of Lipophilicity in the Activity of Hexameric Cyclic Peptoid Ion Carriers. *Eur. J. Org. Chem.* **2021**, *2021*, 464−472.
(64) Groth, P.; Mark, W.; Kenne, L.; Pilotti, A.; Svensson, S.; Swahn, C.-G. Crystal Structure of Cyclopentasarcosyl Dihydrate. *Acta Chem. Scand.* **1973**, *27*, 3419−3426.

https://doi.org/10.1021/acs.jpcb.2c01669
J. Phys. Chem. B 2022, 126, 5161−5174

(65) Vollrath, S. B. L.; Hu, C.; Brase, S.; Kirshenbaum, K. Peptoid Nanotubes: An Oligomer Macrocycle that Reversibly Sequesters Water via Single-Crystal-to-Single-Crystal Transformations. *Chem. Commun.* **2013**, *49*, 2317−2319.
(66) Tedesco, C.; Schettini, R.; Iuliano, V.; Pierri, G.; Fitch, A. N.; De Riccardis, F.; Izzo, I. Role of Side Chains in the Solid State Assembly of Cyclic Peptoids. *Cryst. Growth Des.* **2019**, *19*, 125−133.
(67) Herlan, C. N.; Sommer, K.; Weis, P.; Nieger, M.; Bräse, S. Structural Diversity of Peptoids: Tube-Like Structures of Macrocycles. *Molecules* **2021**, *26*, 150.
(68) Ueno, K.; Shimizu, T. Crystal Structure and Conformation of A Cyclic Tetrapeptide Cyclo(L-Pro-Sar)2 Containing All-cis Peptide Units. *Biopolymers* **1983**, *22*, 633−641.
(69) Northrup, J. D.; Wiener, J. A.; Hurley, M. F. D.; Hou, C.-F. D.; Keller, T. M.; Baxter, R. H. G.; Zdilla, M. J.; Voelz, V. A.; Schafmeister, C. E. Metal-Binding Q-Proline Macrocycles. *Journal of Organic Chemistry* **2021**, *86*, 4867−4876.
(70) Shimizu, T.; Ueno, K.; Tanaka, Y.; Tsuda, K. Ring Conformation of Cyclic Octapeptide Cyclo (L -Pro-Sar)4 in the Crystalline State. *International Journal of Peptide and Protein Research* **1983**, *22*, 231−238.
(71) Groth, P.; Mark, W.; Kenne, L.; Pilotti, A.; Svensson, S.; Swahn, C.-G. Crystal Structure of Cyclooctasarcosyl. *Acta Chem. Scand.* **1973**, *27*, 3217−3226.
(72) Dellwo, M. J.; Wand, A. J. Model-Independent and Model-Dependent Analysis of the Global and Internal Dynamics of Cyclosporin A. *J. Am. Chem. Soc.* **1989**, *111*, 4571−4578.
(73) Groth, P.; Søtofte, I.; Koskinen, R.; Pohjonen, M.-L.; Koskikallio, J. Crystal Conformation of Cyclodecasarcosyl.4CH_3OH at −160°C. *Acta Chem. Scand.* **1976**, *30a*, 840−842.
(74) Rohl, C. A.; Strauss, C. E. M.; Misura, K. M. S.; Baker, D. *Methods Enzymol.* **2004**, *383*, 66−93.

https://doi.org/10.1021/acs.jpcb.2c01669
J. Phys. Chem. B 2022, 126, 5161−5174